

Chapter 2

Linear-Scaling DFT + U for Large Strongly-Correlated Systems

Electronic correlation effects, perhaps even more so than large system sizes, have long captivated electronic structure theorists. In this chapter, we seek to tackle both challenges simultaneously, detailing and demonstrating a linear-scaling implementation of an efficacious ab initio method for strongly-correlated materials.

Specifically, we begin by describing the physics of strongly-correlated systems and we discuss the difficulties experienced, and their origins, when exchange-correlation (XC) functionals of the local density approximation type are applied to such materials.

We describe the popular Density Functional Theory + Hubbard model (DFT + U) method for overcoming these difficulties, briefly discussing its historical development and motivating it as a corrective idempotency penalty functional of a type frequently employed in linear-scaling DFT methods.

We detail an implementation of DFT + U for which the computational effort for calculation of the ground state energy and forces scales linearly with system size. Expressions for optimising the density and ionic positions are derived in full and in a manner which is applicable to any ab initio approach which employs a set of spatially localised, possibly nonorthogonal, functions to represent the single-particle density matrix. We assume no specific form for the projectors used to define the correlated subspaces in DFT + U and include the necessary adaptations to allow for their nonorthogonality.

2.1 Strongly-Correlated Systems

The routine ab initio study of strongly correlated systems, that is those for which the accurate description of the physics is beyond the capacity of band-structure methods such as the unrestricted Hartree–Fock approximation [1], or, somewhat less strictly-speaking, Kohn–Sham DFT [2, 3] within local or semi-local approximations to the XC functional, remains a challenge for electronic structure calculations.

The physics of localised electrons bound to first-row transition metal or lanthanoid ions in such systems is important for understanding and harnessing the behaviour

of complex systems such as molecular magnets [4], inorganic catalysts [5] and the organometallic molecules that facilitate some of the most critical chemical reactions in biochemistry [6]. Indeed, it is often such physics which is central to the interesting functionality of such materials.

Despite its success at predicting ground-state properties of materials, Kohn–Sham DFT [2, 3] fails to describe the physics of such strongly correlated systems when local or semi-local XC functionals are used, often predicting results that are not only quantitatively but qualitatively inconsistent with experiment.

One example of such a failure is the case of Mott–Hubbard insulating solids [7], characterised by narrow bands of $3d$ or $4f$ orbital character adjacent to the Fermi level; the LSDA [8] may badly underestimate local magnetic moments and may even predict a non-zero density of states at the Fermi level [9, 10].

In order to understand the origin of this deficiency, not least because it serves to motivate the DFT + U method, let us consider the renowned Hubbard model [11–13] for strongly correlated fermionic systems. The Hubbard Hamiltonian is usually written in terms of Fermionic creation, $c_m^{(\sigma)\dagger}$, and annihilation, $c_m^{(\sigma)}$, operators, where it is defined as

$$\begin{aligned} \hat{H}^{(\sigma)} = & \sum_{mm'} t_{mm'} c_m^{(\sigma)\dagger} c_{m'}^{(\sigma)} \\ & + \frac{1}{2} \sum_{mm'm''m'''} U_{mm'm''m'''} c_m^{(\sigma)\dagger} c_{m'}^{(-\sigma)\dagger} c_{m'''}^{(-\sigma)} c_{m''}^{(\sigma)}, \end{aligned} \quad (2.1)$$

the indices $\{m\}$ labelling sites in which the electrons, with spin index σ , may reside.

In a continuum model for a real strongly-correlated system, it is useful to use a spatially localised set of single-particle basis orbitals $\{\varphi_m\}$, which we assume here to be spin-independent, with which the creation and annihilation operators, respectively, are spatially resolved via replacement by field operators as per

$$\hat{c}^{(\sigma)}(\mathbf{r}) = \sum_m \varphi_m(\mathbf{r}) c_m^{(\sigma)}, \quad \text{and} \quad \hat{c}^{(\sigma)\dagger}(\mathbf{r}) = \sum_m \varphi_m^*(\mathbf{r}) c_m^{(\sigma)\dagger}. \quad (2.2)$$

These basis orbitals may, for example, take the form of Wannier functions constructed from a linear-combination of Bloch states, as described in [Chap. 1](#). Here we assume that the basis is orthonormal, but the generalisation to the nonorthogonal case is available [14].

In the Hubbard model, the Coulomb repulsion between electrons is introduced by the Hubbard U parameter, that is in its orbitally-decomposed form

$$U_{mm'm''m'''} = \int d\mathbf{r} \int d\mathbf{r}' \varphi_m^*(\mathbf{r}) \varphi_{m'}^*(\mathbf{r}') \hat{v}(\mathbf{r}, \mathbf{r}') \varphi_{m''}(\mathbf{r}) \varphi_{m'''}(\mathbf{r}').$$

For a given form of interaction $\hat{v}(\mathbf{r}, \mathbf{r}')$, the Hubbard U introduces an energy penalty for occupying nearby orbitals and thus correlates the behaviour of different electrons. The factor of one-half eliminates double-counting over pairs of electrons.

The tendency for the electrons to delocalise, by minimising their kinetic energy, is governed by the simple hopping term

$$t_{mm'} = \int d\mathbf{r} \varphi_m^*(\mathbf{r}) \left[\frac{1}{2} \nabla^2 + \hat{V}_{ext}(\mathbf{r}) \right] \varphi_{m'}(\mathbf{r}), \quad (2.3)$$

which may also include any externally imposed potential.

We will briefly discuss a very simple approximation to the Hubbard model, applied to a simple geometry. Ignoring all but density-density interactions, i.e., $m = m''$, $m' = m'''$; interactions between electrons on one site, i.e., $m = m'$; nearest-neighbour single-particle same-spin hopping terms only, where $m' = m \pm 1$ in one dimension; and identical interaction strengths on each site, we simplify the Hamiltonian to

$$\hat{H}^{(\sigma)} = -t \sum_{\langle mm' \rangle} c_m^{(\sigma)\dagger} c_{m'}^{(\sigma)} + \frac{1}{2} U \sum_m \hat{n}_m^{(\sigma)} \hat{n}_m^{(-\sigma)}. \quad (2.4)$$

Here $\hat{n}_m^{(\sigma)} = c_m^{(\sigma)\dagger} c_m^{(\sigma)}$ measures the occupation of site m with an electron of spin σ and the Pauli principle excludes double-occupancy by electrons with identical spins.

Let us apply this model to a periodic chain of sites, for example a one-dimensional chain of s -orbitals or Hydrogen atoms. We may consider two limits. In the limit of $U \ll t$, where correlation effects are weak or the atoms lie close together, the reduction of the kinetic energy is the dominant factor and the low-energy eigenstates are made up of delocalised linear combinations of the basis orbitals. There is no strong distinction between the energy terms acting on occupied and unoccupied levels and there is a continuum of states crossing the Fermi level. At the opposite limit, where the Hubbard U or inter-atomic spacing are large, so that $U \gg t$, the minimisation of orbital double occupancy is paramount, the eigenstates become spatially localised on their basis orbitals. In this case, at half-filling, an energy gap of approximately $U \approx I - A$, where, respectively, I and A are the ionisation potential and binding affinity of hydrogen, opens between the occupied and unoccupied levels, in the same way as in a Mott–Hubbard insulator.

Next, let us see how Kohn–Sham DFT may fit into such a framework. The mapping of the interacting many-electron system onto an equivalent system of noninteracting fermions, which are subject an effective single-particle potential, is central to periodic band-structure methods such as Kohn–Sham DFT. In the language of the Hubbard model, we would write the hopping matrix elements of the Kohn–Sham Hamiltonian as

$$t_{mm'}^{DFT} = \int d\mathbf{r} \psi_m^*(\mathbf{r}) \left[\frac{1}{2} \nabla^2 + \hat{V}_{ext}(\mathbf{r}) + \hat{V}_{Hxc}[n](\mathbf{r}) \right] \psi_{m'}(\mathbf{r}), \quad (2.5)$$

where, in fact, the hopping term makes up the Hamiltonian entirely.

The use of mean-field approximations for the effective potential, $\hat{V}_{Hxc}[n](\mathbf{r})$, such as the LSDA [8], is appropriate and highly successful in systems where the magnitude of the electron’s kinetic energy is large compared with that of the Coulomb

interaction between them, so that $U \ll t$ in which case the neglect of explicit Coulomb correlations is justified. In such systems, usually comprising elements whose $3d$ or $4f$ atomic-like states are either completely empty or filled, the electrons are said to be delocalised, or itinerant in extended systems, and are only scattered weakly by atomic centres.

In strongly correlated systems such as Mott–Hubbard insulators, however, the low-dispersion electrons associated with partial occupation of the aforementioned localised $3d$ or $4f$ atomic orbitals do not fall in the regime of $U \ll t$. The LSDA may thus be found to be severely lacking in accuracy due to its lack of explicit Coulomb correlations.

It is clear that within such simple mean-field band-theories, returning to our simple example, that the hydrogen chain spuriously remains metallic as we increase the inter-atomic distance, retaining a diminishing, though finite, density of states at the Fermi level.

The origin of this apparent failure has been understood since the work of Perdew et al. [15] and is related to the unphysical curvature of the energy functional with respect to electronic occupation number [16–18] inherent to LSDA-type functionals unless a self-interaction correction is employed [19]. In the following section, we describe the DFT + U method that, depending on how we wish to look upon it, reintroduces explicit Coulomb interactions to the Kohn–Sham Hamiltonian or reintroduces the appropriate derivative discontinuity to the XC functional.

2.2 The DFT + U Method

A number of sophisticated methods to correct the description of strong correlation effects within Kohn–Sham DFT have been developed which provide a good compromise between accuracy and computational expense. Many of these methods, notably DFT + Hubbard U (DFT + U) [20, 21] and DFT + dynamical mean field theory (DFT + DMFT) [22, 23] for static and dynamical spatially localised Coulomb correlation effects, respectively, share a common history and conceptual motivation which is based on the Hubbard model we have discussed. In such methods, the electronic system is subdivided into a set of spatially localised correlated subspaces and the remainder which acts as a bath for particle exchange. The description of the strong Coulomb interactions, i.e., $U \geq t$, between particles in the correlated subspaces is deemed to be beyond the capacity of the XC functional, so that explicit supplementation using the Hubbard model is required. In the remainder of the system, the kinetic energy is supposed to be large relative to Coulomb interaction, i.e., $U \ll t$, and the XC functional is assumed to perform adequately. In this manner, a Hubbard model interaction may be used to augment the description of the screened Coulomb interactions in the correlated subspaces while retaining the computationally inexpensive mean-field model for the free-electron like remainder of the system.

Figure 2.1 illustrates, as an example, a spatially delocalised single-particle orbital, $\psi_n(\mathbf{r})$, together with a localised Wannier function (technically an NGWF), $\phi_m(\mathbf{r})$,

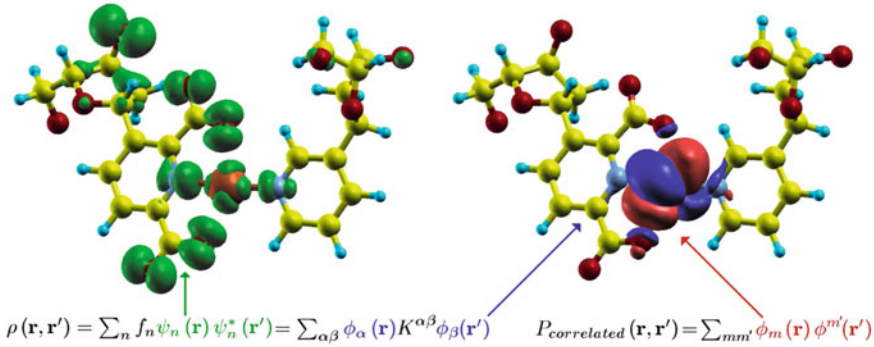


Fig. 2.1 Detail of a Cu^{2+} -mediated DNA base pair [24] in the system on the right of Fig. 1.1, showing the delocalised highest occupied majority-spin molecular orbital (*left*) for comparison with a localised NGWF of localised $3d$ -orbital character (*right*)

used to represent it in an artificial molecular system of technological interest. The description of the Coulomb interactions within the partially filled $\text{Cu}^{2+}(3d)$ sub-shell of such systems may benefit from the use of DFT + U .

We will henceforth describe the orbitals used to delineate the strongly correlated subspaces as *Hubbard projectors*. These are typically spatially localised on a particular transition-metal or lanthanoid atom and usually, but not necessarily, of the same number per correlated site as the number of orbitals, $2l^{(I)} + 1$, in the most localised hydrogenic valence sub-shell of the atom at that site, e.g., we use five Hubbard projectors for a $3d$ sub-shell. Localised Wannier functions built from the Kohn–Sham eigenfunctions may offer an efficient set of Hubbard projectors, and we discuss this possibility further in Chap. 3 and Ref. [25].

In DFT + U , consistency between the subspaces and the bath is provided by ensuring that the electronic density-matrix for the complete system remains subject to the usual requirements of idempotency, compatibility with the ground-state Hamiltonian and proper normalisation. In DFT + DMFT, on the other hand, self-consistency over the density is not routinely enforced at present, although successful examples of such calculations have been demonstrated [26]. The equivalence of the correlated subspace Green’s functions and the projection of the full Green’s function onto these subspaces is, however, required.

Generally for these methods, the occupancy matrix of each correlated subspace is the object which provides, for a given set of Hubbard U parameters which may or may not depend on the density and its response, the necessary information on the electronic density-matrix to the Hubbard model which describes intra-subspace interactions. In Chap. 3, published in Ref. [25], we will describe a self-consistent method for delineating the correlated subspaces based on Wannier functions; in Chap. 4, published in Ref. [27], we discuss the definition of subspace occupancy matrices when using nonorthogonal projector functions; and in Chap. 7 we address the computation of the Hubbard U parameters in the nonorthogonal formalism.

Let us restrict ourselves initially, for simplicity, to the case of orthonormal Hubbard projectors labelled $\{m\}$ at correlated site I , for which the occupancy matrix of spin σ electrons is given by

$$n_{mm'}^{(I)(\sigma)} = Tr \left[c_{m'}^{(I)\dagger} c_m^{(I)\dagger} \hat{\rho}^{(\sigma)} \right] = \langle \varphi_m^{(I)} | \hat{\rho}^{(\sigma)} | \varphi_{m'}^{(I)} \rangle. \quad (2.6)$$

Considering, as our starting point, the first rotationally-invariant form of DFT + U introduced in the literature, that of Refs. [28, 29] and known as LSDA + U . In this method, the correlation, classical Coulomb repulsion and exchange parts of the fermionic Hubbard Hamiltonian, Eq. 2.1, are expressed separately for each spatially localised correlated subspace. The trace of these interaction terms with the appropriate occupancy matrices gives the energy expectation value of the Hubbard Hamiltonian, for each subspace, with the Kohn–Sham density-matrix.

Summation over correlated sites and the electron spin index gives the energy correction due to explicit Coulomb interactions for this density-matrix, which is given by

$$E_U = \frac{1}{2} \sum_{I\sigma\{m\}} \left\{ U_{mm''m'm'''}^{(I)} n_{mm'}^{(I)(\sigma)} n_{m''m'''}^{(I)(-\sigma)} + \left(U_{mm''m'm'''}^{(I)} - U_{mm''m''m'}^{(I)} \right) n_{mm'}^{(I)(\sigma)} n_{m''m'''}^{(I)(\sigma)} \right\}. \quad (2.7)$$

Here, the first, second and third terms correspond, respectively, to spin off-diagonal density-density repulsion (correlation), spin-diagonal density-density repulsion and spin-diagonal exchange effects. If unscreened Coulomb interactions are used to build the Hubbard U parameters, this is the Hartree-Fock approximation to the Coulomb energy of the correlated subspaces.

The contribution to the DFT energy functional arising from the correlated subspaces and already included in the conventional exchange correlation term in a mean-field sense must be subtracted in order to approximately remove double-counting of the Coulomb interactions. The DFT + U energy functional is thus generally given by

$$E_{DFT+U} = E_{DFT} + E_U - E_{DC}. \quad (2.8)$$

The double-counting term used in this rotationally-invariant form of LSDA + U model is the simple “atomic limit” approximation detailed in Ref. [30], calculated by presupposing an integer occupancy of the correlated subspaces and thus given by

$$E_{DC} = \frac{1}{2} \sum_{I\sigma} \left\{ U^{(I)} N^{(I)(\sigma)} \left(\sum_{\sigma'} N^{(I)(\sigma')} - 1 \right) - J^{(I)} N^{(I)(\sigma)} \left(N^{(I)(\sigma)} - 1 \right) \right\}. \quad (2.9)$$

Here, the total occupancy for a given site and spin and subspace-averaged Coulomb repulsion and spin-diagonal exchange parameters are denoted, respectively, by

$$N^{(I)(\sigma)} = \sum_m N_{mm}^{(I)(\sigma)}, \quad (2.10)$$

$$U^{(I)} = \frac{1}{(2l^{(I)} + 1)^2} \sum_{m,m'} U_{mm'mm'}^{(I)} \quad \text{and} \quad (2.11)$$

$$J^{(I)} = \frac{1}{(2l^{(I)}) (2l^{(I)} + 1)} \sum_{m,m' \neq m} U_{mm'm'm}^{(I)}. \quad (2.12)$$

Alternative forms of the double-counting correction, such as those described in Refs. [20, 31], are also available although we do not discuss them further.

Following Ref. [16], which offers a simplified rotationally-invariant DFT + U functional which itself is based on previous proposals in Ref. [10], we next neglect the corrections associated with exchange effects and with interactions between electrons of different spin. Some manipulation allows us to re-write the DFT + U correction, in this approximation, as

$$E_{DFT+U} = \frac{1}{2} \sum_{I\sigma} \left\{ \sum_{mm'} U_{mm'mm'}^{(I)} \left(n_{mm}^{(I)(\sigma)} n_{m'm'}^{(I)(\sigma)} - n_{mm'}^{(I)(\sigma)} n_{m'm}^{(I)(\sigma)} \right) - U^{(I)} N^{(I)(\sigma)} \left(N^{(I)(\sigma)} - 1 \right) \right\} \quad (2.13)$$

$$= \frac{1}{2} \sum_{I\sigma} \sum_{mm'} \left\{ \left(U_{mm'mm'}^{(I)} - U^{(I)} \right) n_{mm}^{(I)(\sigma)} n_{m'm'}^{(I)(\sigma)} + U^{(I)} n_{mm'}^{(I)(\sigma)} \delta_{mm'} - U_{mm'mm'}^{(I)} n_{mm'}^{(I)(\sigma)} n_{m'm}^{(I)(\sigma)} \right\}. \quad (2.14)$$

Finally, we may simplify this further by approximating the orbitally-decomposed $U_{mm'mm'}^{(I)}$ by its average scalar $U^{(I)}$, in which case the first term in Eq. 2.14 vanishes to give the widely-used simplified DFT + U functional

$$E_{DFT+U} = \frac{1}{2} \sum_{I\sigma} \sum_{mm'} U^{(I)} \left(n_{mm'}^{(I)(\sigma)} \delta_{mm'} - n_{mm'}^{(I)(\sigma)} n_{m'm}^{(I)(\sigma)} \right) = \frac{1}{2} \sum_{I\sigma} \sum_m U^{(I)} \left(n_{mm}^{(I)(\sigma)} - \sum_{m'} n_{mm'}^{(I)(\sigma)} n_{m'm}^{(I)(\sigma)} \right). \quad (2.15)$$

The interaction averaging approximation, which is expected to be most valid for a spherically symmetric correlated subspace immersed in an isotropic environment,

$$U_{mm'mm'}^{(I)} \approx U^{(I)}, \quad \forall m, m' \in \{1, \dots, 2l^{(I)} + 1\}, \quad (2.16)$$

might suggest that we may alternatively replace the scalar approximation $U^{(I)}$ by its orbital dependent counterpart in Eq. 2.14. This also gives a rather simple DFT + U functional,

$$E_{\text{DFT}+U} = \frac{1}{2} \sum_{I\sigma} \sum_{mm'} U_{mm'mm'}^{(I)} \left(n_{mm}^{(I)(\sigma)} \delta_{mm'} - n_{mm'}^{(I)(\sigma)} n_{m'm}^{(I)(\sigma)} \right),$$

however it is not of practical utility since it is not invariant under unitary rotations among the Hubbard projectors. We return to the question of constructing tensorially valid DFT + U corrections with orbital-dependent parameters in Chap. 7.

The principal effect of the DFT + U correction Eq. 2.15 is to approximately emulate the exact XC functional by introducing a derivative discontinuity in the total-energy with respect to the occupancy matrix of the correlated subspaces at integer values. The DFT + U correction to the Kohn–Sham potential, given by

$$\hat{V}_{\text{DFT}+U} = \sum_{I\sigma} \sum_{mm'} U^{(I)} |\varphi_m^{(I)}\rangle \left(\frac{1}{2} \delta_{mm'} - n_{mm'}^{(I)(\sigma)} \right) \langle \varphi_{m'}^{(I)}|, \quad (2.17)$$

acts to restore the correct occupancy dependence of the potential, and is attractive or repulsive for occupancy-matrix elements greater or less than one-half, respectively. The result, to a first approximation, is the penalisation of non-integer correlated subspace occupancies and, consequently, an opening of an energy gap of order U between the occupied and unoccupied Kohn–Sham states which have a large overlap with the Hubbard projectors, thus facilitating the simulation of strongly-correlated systems such as Mott–Hubbard insulators within Kohn–Sham DFT.

The DFT + U correction to the energy functional allows a simple interpretation, or perhaps motivation, as an idempotency penalty-functional [32] of the type often used to maintain the idempotency of the Kohn–Sham density-matrix in linear-scaling DFT. Assuming that the particles occupying the correlated subspaces interact strongly with each other, compared to their interaction with the bath, each subspace effectively acts as an individual open quantum system. As such, we could separately impose the density-matrix idempotency condition, i.e., Fock antisymmetry, of the projected density-matrix for each subspace.

However, the idempotency of the density-matrix for the complete Kohn–Sham system is a condition which must be exactly satisfied, at the ground-state, and the idempotency of each subspace density-matrix is, in general, a competing condition. Thus, the subspace idempotency may be only partially enforced up to an idempotency functional of the form

$$\sum_{I\sigma} \text{Tr} \left[\lambda^{(I)(\sigma)} \left(\hat{n}^{(I)(\sigma)} - \hat{n}^{(I)(\sigma)2} \right) \right]; \quad \lambda^{(I)(\sigma)} = \frac{U^{(I)(\sigma)}}{2}, \quad (2.18)$$

which penalises the degradation of fermionic behaviour in each correlated subspace. Since the strength of the effective Coulomb interactions is closely related to the extent

to which the derivative discontinuity is lacking in the XC functional, and the latter is responsible for the spurious partial-occupancy of localised states (or correlated subspace idempotency deviation) by that functional, the Hubbard U parameter may be heuristically identified with the pre-factor of the idempotency penalty-functional.

2.3 Framework for Linear-Scaling DFT + U

We now proceed to describe the implementation of the DFT + U functional defined by Eq. 2.15 in a contemporary approach to linear-scaling DFT. Firstly, in this section, we establish a notational framework for expressing the Hubbard projectors, which are permitted to be nonorthogonal for each correlated subspace, in terms of a localised nonorthogonal set of support functions of the type typically used to represent the Kohn–Sham density matrix in many linear-scaling approaches.

Due to the spatial localisation of both the Hubbard projectors and the support functions, matrix sparsity patterns naturally play an important role in the construction of our linear-scaling DFT + U method. In fact, as we will show, matrix sparsity patterns allow us to carry out DFT + U calculations involving a large number of correlated subspaces in a very efficient manner.

We will make due comment on matrix sparsity issues, when appropriate, as we describe the elements of our linear-scaling implementation of DFT + U . Linear scaling with respect to the number of correlated subspaces in the system may be achieved for some elements of the DFT + U module, and, in less favourable cases, with respect to the total number of atoms in the simulation cell.

We begin by expressing the Hubbard projectors $\{\varphi_m^{(I)}\}$ spanning each correlated subspace I in terms of the nonorthogonal basis functions $\{\phi_\alpha\}$ via the linear transformation

$$\varphi_m^{(I)}(\mathbf{r}) = \phi_\alpha(\mathbf{r}) S^{\alpha\beta} V_{\beta m}^{(I)}. \quad (2.19)$$

Here, we must assume that the Hubbard projectors are fully expandable in the frame of their surrounding NGWFs, though this does not introduce any limitation, in practice, since the explicit expansion of the projectors in the *psinc* function basis is used in the update of the NGWFs themselves. We also assume, for notational simplicity, that identical Hubbard projectors are used for each spin channel, although the generalisation to spin-dependent projectors is straightforward.

Here $S^{\alpha\beta} = \langle \phi^\alpha | \phi^\beta \rangle$ is the contravariant metric on the NGWFs, as usual, and it follows that the transformation matrix between covariant basis functions and projectors is given by

$$V_{\beta m}^{(I)} = \langle \phi_\beta | \varphi_m^{(I)} \rangle, \quad (2.20)$$

which may be a very sparse matrix for a low density of correlated subspaces.

It will be convenient to establish the adjoint (once covariant for the support function index and once for the Hubbard projector index) transformation matrix as

$$W_{m\alpha}^{(I)} = V_{\alpha m}^{(I)\dagger} = \langle \varphi_m^{(I)} | \phi_\alpha \rangle. \quad (2.21)$$

The metric on each correlated subspace is discussed in detail in [Chap. 4](#) and Ref. [27]; most of the expressions in this chapter extend readily to the delocalised Hubbard projector duals discussed there. Here, for brevity, we will restrict ourselves to the case of the localised Hubbard projector duals defined by

$$|\varphi^{(I)m}\rangle = |\varphi_{m'}^{(I)}\rangle O_{mm'}^{(I)}; \quad O_{mm'}^{(I)} = \langle \varphi_m^{(I)} | \varphi_{m'}^{(I)} \rangle, \quad (2.22)$$

where an individual metric tensor $O_{\bullet\bullet}^{(I)}$ is used for each correlated subspace, as we propose in [Chap. 4](#) and Ref. [27], in order to maintain the tensorial invariance of the total energy.

The generalised occupation matrix for each correlated subspace, a mixed tensor with respect to the projector indices, is expressed in the support function representation as

$$\begin{aligned} n_m^{(I)(\sigma)m'} &= \langle \varphi_m^{(I)} | \hat{\rho}^{(\sigma)} | \varphi_{m'}^{(I)} \rangle \\ &= \langle \varphi_m^{(I)} | \phi_\alpha \rangle K^{(\sigma)\alpha\beta} \langle \phi_\beta | \varphi_{m''}^{(I)} \rangle O_{m''m'}^{(I)} \\ &= W_{m\alpha}^{(I)} K^{(\sigma)\alpha\beta} V_{\beta m''}^{(I)} O_{m''m'}^{(I)} \\ &= \left(W^{(I)} K^{(\sigma)} V^{(I)} O^{(I)} \right)_m^{m'}, \end{aligned} \quad (2.23)$$

where

$$K^{(\sigma)\alpha\beta} = \sum_{i\mathbf{k}} M^{(\sigma)\alpha}_{i\mathbf{k}} f_{i\mathbf{k}}^{(\sigma)} (M^{(\sigma)\dagger})_{i\mathbf{k}}^\beta \quad (2.24)$$

is the density kernel relating support functions (assumed to be spin-independent) to Kohn–Sham orbitals via a linear transformation matrix $M^{(\sigma)\alpha}_{i\mathbf{k}} = \langle \phi^\alpha | \psi_{i\mathbf{k}}^{(\sigma)} \rangle$.

The DFT+ U correction to the total energy, in the case of a generalised spin-dependent two-index interaction tensor $U_m^{(I)(\sigma)m'}$ (approximations for the interaction tensor of various rank are discussed in [Chap. 7](#)), is generally computed using the matrix trace

$$\begin{aligned} E_{\text{DFT}+U} &= \sum_{I,\sigma} \frac{1}{2} U_m^{(I)(\sigma)m'} \left[n_{m'}^{(I)(\sigma)m''} \left(\delta_{m''}^m - n_{m''}^{(I)(\sigma)m} \right) \right] \\ &= \sum_{I,\sigma} \frac{1}{2} \text{Tr} \left[U^{(I)} W^{(I)} K^{(\sigma)} V^{(I)} O^{(I)} \right. \\ &\quad \left. \times \left(1 - W^{(I)} K^{(\sigma)} V^{(I)} O^{(I)} \right) \right], \end{aligned} \quad (2.25)$$

where here, with further examples to follow, we use multiple continued lines within braces to describe lengthy scalar expressions.

Of course, it is undesirable, both from the point of view of implementation and computational efficiency, to explicitly use separate $V^{(I)}$, $W^{(I)}$ and $O^{(I)}$ matrices for each site. This requires individual matrix products to be carried out for each site before the sum over sites is computed. If care is taken, however, we may safely embed all of these small matrices into large, very sparse, V , W and O matrices for the entire system. These large matrices then fit seamlessly into the hierarchical, parallelised, sparse algebra routines found in a modern linear-scaling DFT code such as ONETEP.

Let us analyse this strategy in greater detail, taking as an example the computation of the occupancy matrix

$$n_{m}^{(I)(\sigma)m'} = W_{m\alpha}^{(I)} K^{(\sigma)\alpha\beta} V_{\beta m''}^{(I)} O^{(I)m''m'}. \quad (2.26)$$

Working from right to left and temporarily placing a site index before each projector index to clarify its meaning, first consider the product

$$(VO)_{\beta}^{(I)m'} = \sum_J V_{\beta(J)m''} O^{(\delta_{JI}J)m''(I)m'} = V_{\beta(I)m''} O^{(I)m''(I)m'}, \quad (2.27)$$

which retains the same sparsity pattern as V due to the block-sparsity of the O matrix (the size of each block is the number of projectors spanning the subspace on the site in question).

Next, taking the product from the left with the density kernel,

$$(KVO)^{(\sigma)\alpha(I)m'} = K^{(\sigma)\alpha\beta} (VO)_{\beta}^{(I)m'}, \quad (2.28)$$

we see that this too has the same sparsity as V when no density kernel truncation is applied, in which case the indices α and β run over all NGWFs. When kernel truncation is enforced, however, the number of values which α can take is reduced and the effort needed for the sum over β is diminished.

Only on the final step, where we compute

$$n_{(J)m}^{(\sigma)(I)m'} = W_{(J)m\alpha} (KVO)^{(\sigma)\alpha(I)m'}, \quad (2.29)$$

do we accumulate extraneous information on the off-site non-locality of the density matrix. Were we to compute this matrix in full and then consider its square, for example, we would find that

$$\sum_K n_{(I)m}^{(\sigma)(K)m''} n_{(K)m''}^{(\sigma)(I)m'} \neq n_m^{(\sigma)(I)m'} n_m^{(\sigma)(I)m'}. \quad (2.30)$$

The former is what is generated in the matrix product, while the latter is what we require. This problem is resolved by explicitly truncating the required occupancy matrix

$$n_{(I)m}^{(\sigma)(I)m'} = W_{(I)m\alpha} (KVO)^{(\sigma)\alpha(I)m'} \quad (2.31)$$

to the same sparsity pattern as O (which is also the same as that of U), thus eliminating any unwanted off-site occupancies. In practice, the unnecessary elements are never actually computed, and no wasted effort is incurred, since the sparse algebra system takes into consideration the sparsity pattern of the product matrix.

2.4 Variations with Respect to the Density Kernel

In the ONETEP code, and indeed most current linear-scaling DFT methods, the LNVD [33–35] technique, described in Chap. 1, is used to minimise the energy with respect to the density-matrix, bringing it closer to commutativity with the Kohn–Sham Hamiltonian while simultaneously driving it towards idempotency. This takes place in the inner energy minimisation loop in ONETEP, where the NGWFs are kept fixed and a non-linear conjugate gradients minimisation of the energy with respect to the matrix elements of the LNVD auxiliary density kernel, $L^{(\sigma)\alpha\beta}$, is carried out.

The Kohn–Sham density kernel is related to the auxiliary density kernel via one iteration of the McWeeny purification transform, i.e.,

$$K^{(\sigma)\alpha\beta} = (3LSL - 2LSLSL)^{(\sigma)\alpha\beta}. \quad (2.32)$$

In our treatment of DFT + U , we go a step further and provide the more general expressions needed for the HSMP [36] adaptation of the LNVD method, in which a density kernel $\tilde{K}^{(\sigma)}$ is expressed as a purified and normalised auxiliary density kernel, explicitly

$$\tilde{K}^{(\sigma)\alpha\beta} = \frac{K^{(\sigma)\alpha\beta} N^{(\sigma)}}{K^{(\sigma)\gamma\delta} S_{\delta\gamma}} = \frac{(3LSL - 2LSLSL)^{(\sigma)\alpha\beta} N^{(\sigma)}}{(3LSL - 2LSLSL)^{(\sigma)\gamma\delta} S_{\delta\gamma}}, \quad (2.33)$$

where $N^{(\sigma)}$ is the correct occupancy of spin channel σ . The kernel renormalisation introduces terms in the gradient akin to a chemical potential, which project out any first-order changes to the electron number, driving the density kernel $\tilde{K}^{(\sigma)}$ towards both normalisation and idempotency as the energy is minimised.

To locate the doubly-covariant derivative of the DFT + U energy term with respect to the auxiliary density kernel, stressing that it is computed strictly using the purified and renormalised density kernel, we make use of the chain-rule for matrix derivatives to write (suppressing the spin index for concision)

$$\frac{\partial E_{DFT+U}}{\partial L^{\alpha\beta}} = \frac{\partial E_{DFT+U}}{\partial K^{\iota\kappa}} \frac{\partial K^{\iota\kappa}}{\partial L^{\alpha\beta}}. \quad (2.34)$$

It may be readily shown that the latter term is given by

$$\begin{aligned} \frac{\partial K^{\iota\kappa}}{\partial L^{\alpha\beta}} = & 3 \left(\delta_{\alpha}^{\iota} S_{\beta\gamma} L^{\gamma\kappa} + L^{\iota\gamma} S_{\gamma\alpha} \delta_{\beta}^{\kappa} \right) \\ & - 2 \left(\begin{aligned} & \delta_{\alpha}^{\iota} S_{\beta\gamma} L^{\gamma\eta} S_{\eta\xi} L^{\xi\kappa} \\ & + L^{\iota\gamma} S_{\gamma\alpha} S_{\beta\eta} L^{\eta\kappa} + L^{\iota\gamma} S_{\gamma\eta} L^{\eta\xi} S_{\xi\alpha} \delta_{\beta}^{\kappa} \end{aligned} \right). \end{aligned} \quad (2.35)$$

The derivative of the DFT + U energy term with respect to the purified density kernel $K^{\bullet\bullet}$ may be broken into products of derivatives and rearranged as follows

$$\begin{aligned}
\frac{\partial E_{DFT+U}}{\partial K^{\iota\kappa}} &= \frac{\partial}{\partial \tilde{K}^{\eta\theta}} \left[E_{DFT+U} \left(\tilde{K}^{\bullet\bullet} \right) \right] \frac{\partial \tilde{K}^{\theta\eta}}{\partial K^{\iota\kappa}} \\
&= H_{\eta\theta}^{DFT+U} \frac{\partial}{\partial K^{\iota\kappa}} \left[\frac{N}{K^{\alpha\beta} S_{\beta\alpha}} K^{\theta\eta} \right] \\
&= H_{\eta\theta}^{DFT+U} \frac{N}{(K^{\alpha\beta} S_{\beta\alpha})^2} \left[\frac{\partial K^{\theta\eta}}{\partial K^{\iota\kappa}} (K^{\gamma\delta} S_{\delta\gamma}) - K^{\theta\eta} S_{\iota\kappa} \right] \\
&= H_{\eta\theta}^{DFT+U} \frac{N}{(K^{\alpha\beta} S_{\beta\alpha})} \left[\delta_{\theta}^{\iota} \delta_{\eta}^{\kappa} - \frac{K^{\theta\eta}}{(K^{\gamma\delta} S_{\delta\gamma})} S_{\iota\kappa} \right]. \tag{2.36}
\end{aligned}$$

We may next write the gradient with respect to the density kernel in terms of a preconditioned contribution to the Hamiltonian, denoted by $\tilde{H}_{\bullet\bullet}^{DFT+U}$, identifying the DFT+ U correction to the chemical potential needed to preserve the electron number of the system as

$$\mu^{DFT+U} = \frac{H_{\eta\theta}^{DFT+U} K^{\theta\eta}}{(K^{\gamma\delta} S_{\delta\gamma})}, \tag{2.37}$$

since

$$\begin{aligned}
\frac{\partial E_{DFT+U}}{\partial K^{\iota\kappa}} &= \frac{N}{(K^{\alpha\beta} S_{\beta\alpha})} \left[H_{\iota\kappa}^{DFT+U} - \frac{H_{\eta\theta}^{DFT+U} K^{\theta\eta}}{(K^{\gamma\delta} S_{\delta\gamma})} S_{\iota\kappa} \right] \\
&= \frac{N}{(K^{\alpha\beta} S_{\beta\alpha})} \left[H_{\iota\kappa}^{DFT+U} - \mu^{DFT+U} S_{\iota\kappa} \right] \\
&= \frac{N}{(K^{\alpha\beta} S_{\beta\alpha})} \tilde{H}_{\iota\kappa}^{DFT+U}. \tag{2.38}
\end{aligned}$$

The DFT+ U contribution to the Hamiltonian, used in the above and which is computed using the purified and renormalised density kernel, in practice is given by

$$\begin{aligned}
H_{\iota\kappa}^{DFT+U} &= \frac{\partial E_{DFT+U}}{\partial K^{\iota\kappa}} \\
&= \sum_I \frac{1}{2} U_{m'}^{(I)m} \left[\frac{\partial n_m^{(I)m'}}{\partial K^{\iota\kappa}} - \frac{\partial n_m^{(I)m''}}{\partial K^{\iota\kappa}} n_{m''}^{(I)m'} - n_m^{(I)m''} \frac{\partial n_{m''}^{(I)m'}}{\partial K^{\iota\kappa}} \right]. \tag{2.39}
\end{aligned}$$

In order to express this in terms of the NGWF representation, we begin by noting that the partial derivative of the occupation matrix, for a given subspace, with respect to an arbitrary density kernel $K^{\bullet\bullet}$, is given by

$$\begin{aligned}
\frac{\partial n_m^{(I)m'}}{\partial K^{\iota\kappa}} &= \frac{\partial}{\partial K^{\iota\kappa}} \left[W_{m\gamma}^{(I)} K^{\gamma\delta} V_{\delta m''}^{(I)} O^{(I)m''m'} \right] \\
&= W_{m\gamma}^{(I)} \delta_{\iota}^{\gamma} \delta_{\kappa}^{\delta} V_{\delta m''}^{(I)} O^{(I)m''m'} \\
&= W_{m\iota}^{(I)} V_{\kappa m''}^{(I)} O^{(I)m''m'}. \tag{2.40}
\end{aligned}$$

The trace of this over the Hubbard projectors gives the covariant support function representation of the Hubbard projection for subspace $\mathcal{C}^{(I)}$, that is

$$\sum_m \frac{\partial n_m^{(I)m}}{\partial K_{\iota\kappa}} = V_{\kappa m''}^{(I)} O^{(I)m''m} W_{m\iota}^{(I)} \equiv P_{\kappa\iota}^{(I)}. \quad (2.41)$$

It follows that the products of the occupancy matrix and its derivative, always computed in the frame of Hubbard projectors in practice since there they each have the block-diagonal sparsity pattern of O , are expressed in the support function representation as

$$\begin{aligned} \frac{\partial n_m^{(I)m''}}{\partial K^{(\sigma)\iota\kappa}} n_{m''}^{(I)m'} &= \left(W_{m\iota}^{(I)} V_{\kappa m''}^{(I)} O^{(I)m''m'} \right) \left(W^{(I)} K V^{(I)} O^{(I)} \right)_{m''}^{m'} \\ &= W_{m\iota}^{(I)} \left(P^{(I)} K V^{(I)} O^{(I)} \right)_{\kappa}^{m'} \end{aligned} \quad (2.42)$$

and, taking the complimentary product,

$$\begin{aligned} n_m^{(I)m''} \frac{\partial n_{m''}^{(I)m'}}{\partial K^{(\sigma)\iota\kappa}} &= \left(W^{(I)} K V^{(I)} O^{(I)} \right)_m^{m''} \left(W_{m''\iota}^{(I)} V_{\kappa m''}^{(I)} O^{(I)m''m'} \right) \\ &= \left(W^{(I)} K P^{(I)} \right)_{m\iota} \left(V^{(I)} O^{(I)} \right)_{\kappa}^{m'}. \end{aligned} \quad (2.43)$$

We are free to evaluate the Hubbard U interaction operator as a mixed tensor in the NGWF representation, so that

$$U_{\alpha}^{(I)\gamma} = V_{\alpha m}^{(I)} O^{(I)mm'} U_{m'}^{(I)m''} W_{m''\beta}^{(I)} S^{\beta\gamma}. \quad (2.44)$$

As a result, noting that the Hubbard projection operator and the Hubbard interaction operator commute but that the density-matrix and the Hubbard interaction operator may not, the DFT+ U term in the covariant Hamiltonian, denoted $H_{\bullet\bullet}^{(\sigma)DFT+U}$, is expressed in the support function representation by

$$H_{\alpha\beta}^{(\sigma)DFT+U} = \sum_I \frac{1}{2} \begin{pmatrix} U^{(I)} P^{(I)} \\ -P^{(I)} K^{(\sigma)} U^{(I)} P^{(I)} \\ -U^{(I)} P^{(I)} K^{(\sigma)} P^{(I)} \end{pmatrix}_{\alpha\beta}^{(I)}. \quad (2.45)$$

The DFT+ U term in the total-energy, on the other hand, is succinctly expressed as

$$E_{DFT+U}^{(\sigma)} = \sum_I \frac{1}{2} U_{\alpha}^{(I)\gamma} \left(P^{(I)} K^{(\sigma)} - P^{(I)} K^{(\sigma)} P^{(I)} K^{(\sigma)} \right)_{\gamma}^{\alpha}. \quad (2.46)$$

The associated DFT+ U independent-particle, “band-structure”, energy correction, $E_{DFT+U}^{IP} = H_{\iota\kappa}^{DFT+U} \tilde{K}^{\kappa\iota}$, does not equal the energy term E_{DFT+U} and so the energy

correction entering into the computation of μ^{DFT+U} is not the same as the correction to the total-energy. This explicitly demonstrates that DFT + U is a correction beyond the independent-particle approximation.

The required DFT + U contribution to the covariant gradient is then provided by the product of the preconditioned term in the Hamiltonian and the derivative of the density kernel with respect to its auxiliary counterpart. We find that this is given by (again suppressing the spin index)

$$\begin{aligned} \frac{\partial E_{DFT+U}}{\partial L^{\alpha\beta}} &= \frac{N}{(K^{\gamma\delta} S_{\delta\gamma})} \tilde{H}_{\kappa\iota}^{DFT+U} \frac{\partial K^{\iota\kappa}}{\partial L^{\alpha\beta}} \\ &= \frac{N}{(3LSL - 2LSLSL)^{\gamma\delta} S_{\delta\gamma}} \\ &\quad \times \begin{pmatrix} 3(\tilde{H}LS + SL\tilde{H})_{\alpha\beta} \\ -2(\tilde{H}LSLS + SL\tilde{H}LS + SL\tilde{H})_{\alpha\beta} \end{pmatrix}. \end{aligned} \quad (2.47)$$

Here, $\tilde{H}_{\bullet\bullet}$ is shorthand for the preconditioned DFT + U term in the Hamiltonian and is given by

$$\tilde{H}_{\bullet\bullet}^{DFT+U} = H_{\bullet\bullet}^{DFT+U} - \mu^{DFT+U} S_{\bullet\bullet}. \quad (2.48)$$

Explicitly, we may now write the DFT + U correction to the Hamiltonian as

$$\tilde{H}_{\alpha\beta}^{(\sigma)DFT+U} = \sum_I \frac{1}{2} U_{\eta}^{(I)\zeta} \left[\begin{array}{c} P_{\zeta\beta} (\delta - PK)_{\alpha}^{\eta} - (PKP)_{\zeta\beta}^{\eta} \delta_{\alpha}^{\eta} \\ - (PK - 2PKPK)_{\zeta}^{\eta} S_{\alpha\beta} \\ \times (K^{\gamma\delta} S_{\delta\gamma})^{-1} \end{array} \right]^{(I)(\sigma)}.$$

For a refinement of the auxiliary density kernel $L^{\alpha\beta}$, any update must also be a contravariantly transforming tensor, as noted in Refs. [14, 37]. In order to provide such a search direction, it is necessary that we pre- and post-multiply the above covariant gradient with the contravariant metric tensor on the NGWFs, that is the inverse overlap matrix of the NGWFs at the point at which the gradient itself is computed, to give

$$G_{DFT+U}^{(\sigma)\alpha\beta} = (S^{-1})^{\alpha\gamma} \frac{\partial E_{DFT+U}}{\partial L^{(\sigma)\gamma\delta}} (S^{-1})^{\delta\beta} \quad (2.49)$$

Carrying this out, we obtain the DFT + U contribution to the contravariant density kernel gradient,

$$\begin{aligned} G_{DFT+U}^{(\sigma)\alpha\beta} &= \frac{N}{(3LSL - 2LSLSL)^{\gamma\delta} S_{\delta\gamma}} \\ &\quad \times \begin{pmatrix} 3(S^{-1}\tilde{H}L + L\tilde{H}S^{-1}) \\ -2(S^{-1}\tilde{H}LSL + L\tilde{H}L + LSL\tilde{H}S^{-1}) \end{pmatrix}^{\alpha\beta}, \end{aligned} \quad (2.50)$$

where \tilde{H} is a shorthand for the preconditioned correction to the Hamiltonian given by Eq. 2.48.

2.5 Variations with Respect to the NGWFs

Now that we have shown how to incorporate DFT + U into density-matrix based methods which used a fixed nonorthogonal representation, we turn our attention to the outer energy-minimisation loop in ONETEP. We consider the contribution due to DFT + U of the total-energy variation with respect to the expansion coefficients of the NGWF for a fixed, optimised, density kernel. The results of this section, of course, apply to any technique which optimises its representation functions for minimal energy, such as those described in Refs. [38–41].

The required derivative with respect to covariant support functions may be broken into its contributing parts as

$$\begin{aligned}
 \frac{\partial E_{DFT+U}}{\partial \phi_\gamma(\mathbf{r})} &= \frac{\partial E_{DFT+U}}{\partial \tilde{K}^{\eta\theta}} \left(\frac{\partial \tilde{K}^{\eta\theta}}{\partial K^{\iota\kappa}} \frac{\partial K^{\iota\kappa}}{\partial \phi_\gamma(\mathbf{r})} + \frac{\partial \tilde{K}^{\eta\theta}}{\partial S_{\lambda\nu}} \frac{\partial S_{\lambda\nu}}{\partial \phi_\gamma(\mathbf{r})} \right) \\
 &\quad + \sum_J \frac{\partial E_{DFT+U}}{\partial P_{\xi\tau}^{(J)}} \frac{\partial P_{\xi\tau}^{(J)}}{\partial \phi_\gamma(\mathbf{r})} \\
 &= H_{\theta\eta}^{DFT+U} \left(\frac{\partial \tilde{K}^{\eta\theta}}{\partial K^{\iota\kappa}} \frac{\partial K^{\iota\kappa}}{\partial S_{\lambda\nu}} + \frac{\partial \tilde{K}^{\eta\theta}}{\partial S_{\lambda\nu}} \right) \frac{\partial S_{\lambda\nu}}{\partial \phi_\gamma(\mathbf{r})} \\
 &\quad + \sum_J \frac{\partial E_{DFT+U}}{\partial P_{\xi\tau}^{(J)}} \frac{\partial P_{\xi\tau}^{(J)}}{\partial \phi_\gamma(\mathbf{r})}. \tag{2.51}
 \end{aligned}$$

As for the density kernel gradient, the NGWF gradient is calculated using the purified and renormalised density kernel and so contains a preconditioning term which drives the trace of the density-matrix to the correct occupancy of the system.

The covariant metric explicitly depends on the covariant functions and, assuming real-valued NGWFs for simplicity, we find that

$$\frac{\partial S_{\lambda\nu}}{\partial \phi_\gamma(\mathbf{r})} = \delta_\lambda^\gamma \phi_\nu(\mathbf{r}) + \delta_\nu^\gamma \phi_\lambda(\mathbf{r}). \tag{2.52}$$

The terms in the parentheses of the second to last line of Eq. 2.52 evaluate to

$$\frac{\partial \tilde{K}^{\eta\theta}}{\partial S_{\lambda\nu}} = \frac{N}{(K^{\alpha\beta} S_{\beta\alpha})} \left[-\frac{K^{\eta\theta}}{(K^{\gamma\delta} S_{\delta\gamma})} K^{\lambda\nu} \right], \tag{2.53}$$

$$\frac{\partial \tilde{K}^{\eta\theta}}{\partial K^{\epsilon\zeta}} = \frac{N}{(K^{\alpha\beta} S_{\beta\alpha})} \left[\delta_\epsilon^\eta \delta_\zeta^\theta - \frac{K^{\eta\theta}}{(K^{\gamma\delta} S_{\delta\gamma})} S_{\epsilon\zeta} \right] \text{ and} \tag{2.54}$$

$$\frac{\partial K^{\epsilon\zeta}}{\partial S_{\lambda\nu}} = 3L^{\epsilon\lambda} L^{\nu\zeta} - 2L^{\epsilon\lambda} (LSL)^{\nu\zeta} - 2(LSL)^{\epsilon\lambda} L^{\nu\zeta}. \tag{2.55}$$

Contraction between the DFT+ U term in the Hamiltonian and these terms provide a tensor $\tilde{Q}^{\bullet\bullet}$ which generates the contribution to the NGWF gradient due to mixing among the NGWFs, given by

$$\begin{aligned}\tilde{Q}^{\lambda\nu} &= H_{\theta\eta}^{DFT+U} \left(\frac{\partial \tilde{K}^{\eta\theta}}{\partial K^{\iota\kappa}} \frac{\partial K^{\iota\kappa}}{\partial S_{\lambda\nu}} + \frac{\partial \tilde{K}^{\eta\theta}}{\partial S_{\lambda\nu}} \right) \\ &= \frac{N}{(K^{\alpha\beta} S_{\beta\alpha})} \left(3L\tilde{H}L - 2L\tilde{H}LSL - 2LSL\tilde{H}L - \mu^{DFT+U} K \right)^{\lambda\nu}.\end{aligned}\quad (2.56)$$

The remaining terms involve the Hubbard projections themselves, and changes beyond linear mixing of the NGWFs. We begin with the action of the DFT+ U contribution to the Hamiltonian on the correlated subspace projections, that is

$$\begin{aligned}\frac{\partial E_{DFT+U}}{\partial P_{\xi\tau}^{(J)}} &= \frac{\partial}{\partial P_{\xi\tau}^{(J)}} \left[\sum_I \frac{1}{2} U_{\alpha}^{(I)\gamma} \left(P^{(I)} \tilde{K} - P^{(I)} \tilde{K} P^{(I)} \tilde{K} \right)^{\alpha}_{\gamma} \right] \\ &= \frac{1}{2} U_{\alpha}^{(J)\gamma} \frac{\partial}{\partial P_{\xi\tau}^{(J)}} \left[\left(P^{(J)} \tilde{K} - P^{(J)} \tilde{K} P^{(J)} \tilde{K} \right)^{\alpha}_{\gamma} \right] \\ &= \frac{1}{2} U_{\alpha}^{(J)\gamma} \left(\delta_{\gamma}^{\xi} \tilde{K}^{\tau\alpha} - \delta_{\gamma}^{\xi} \left(\tilde{K} P^{(J)} \tilde{K} \right)^{\tau\alpha} - \left(P^{(J)} \tilde{K} \right)^{\xi}_{\gamma} \tilde{K}^{\tau\alpha} \right) \\ &= \frac{1}{2} \left(\tilde{K} U^{(J)} - \tilde{K} P^{(J)} \tilde{K} U^{(J)} - \tilde{K} U^{(J)} P^{(J)} \tilde{K} \right)^{\tau\xi} \\ &= \tilde{K}^{\tau\epsilon} H_{\epsilon\xi}^{(J)DFT+U} P^{(J)\xi\zeta} = P^{(J)\tau\epsilon} H_{\epsilon\xi}^{(J)DFT+U} \tilde{K}^{\zeta\xi},\end{aligned}\quad (2.57)$$

where $H_{\alpha\beta}^{(J)DFT+U}$ is the contribution from each site in Eq. 2.45. The Hubbard projection operators depend explicitly on the covariant NGWFs which overlap with their corresponding Hubbard projectors (or Hubbard projector duals) and this dependence may be expressed as

$$\begin{aligned}\frac{\partial P_{\xi\tau}^{(J)}}{\partial \phi_{\gamma}(\mathbf{r})} &= \frac{\partial}{\partial \phi_{\gamma}(\mathbf{r})} \left[V_{\xi m'}^{(J)} O^{(J)m'm} W_{m\tau}^{(J)} \right] \\ &= \delta_{\xi}^{\gamma} \varphi_{m'}^{(J)}(\mathbf{r}) O^{(J)m'm} W_{m\tau}^{(J)} + V_{\xi m'}^{(J)} O^{(J)m'm} \varphi_m^{(J)}(\mathbf{r}) \delta_{\tau}^{\gamma},\end{aligned}\quad (2.58)$$

where we have assumed real-valued Hubbard projectors. We may combine the latter two results to compute the remaining DFT+ U term in the NGWF gradient, that is for each site J ,

$$\begin{aligned}\frac{\partial E_{DFT+U}}{\partial P_{\xi\tau}^{(J)}} \frac{\partial P_{\xi\tau}^{(J)}}{\partial \phi_{\gamma}(\mathbf{r})} &= \varphi_{m'}^{(J)}(\mathbf{r}) O^{(J)m'm} W_{m\tau}^{(J)} P^{(J)\tau\epsilon} H_{\epsilon\xi}^{(J)DFT+U} \tilde{K}^{\zeta\gamma} \\ &\quad + \tilde{K}^{\gamma\epsilon} H_{\epsilon\xi}^{(J)DFT+U} P^{(J)\xi\zeta} V_{\xi m'}^{(J)} O^{(J)m'm} \varphi_m^{(J)}(\mathbf{r}) \\ &= 2\tilde{K}^{\gamma\epsilon} H_{\epsilon\xi}^{(J)DFT+U} P^{(J)\xi\zeta} V_{\xi m'}^{(J)} O^{(J)m'm} \varphi_m^{(J)}(\mathbf{r}) \\ &= 2\tilde{K}^{\gamma\epsilon} \left[\hat{H}^{(J)DFT+U} \phi_{\epsilon} \right](\mathbf{r}).\end{aligned}\quad (2.59)$$

Here, due to the subspace-localised nature of the DFT + U correction, only those NGWFs ϕ_ϵ which explicitly overlap with the Hubbard projectors expressed on the grid $\varphi_m^{(J)}$ contribute and thus need to be summed over.

To conclude, the contravariant gradient of the DFT + U energy with respect to the NGWFs is given by the expression

$$\frac{\partial E_{DFT+U}}{\partial \phi_\gamma(\mathbf{r})} = 2 \left[\tilde{Q}^{\gamma\nu} \phi_\nu + \sum_J \tilde{K}^{\gamma\epsilon} \left[\hat{H}^{(J)DFT+U} \phi_\epsilon \right] \right] (\mathbf{r}). \quad (2.60)$$

Since, however, we require a covariantly transforming NGWF update in order to improve upon those functions while preserving their tensorial character, the above contravariant gradient needs to be multiplied with the covariant metric tensor to give the necessary covariant DFT + U NGWF gradient term,

$$g_\alpha(\mathbf{r}) = 2S_{\alpha\gamma} \left[\tilde{Q}^{\gamma\nu} \phi_\nu + \sum_J \tilde{K}^{\gamma\epsilon} \left[\hat{H}^{(J)DFT+U} \phi_\epsilon \right] \right] (\mathbf{r}). \quad (2.61)$$

2.6 Variations with Respect to Ionic Positions

While DFT + U is less commonly applied as a method to improve first-principles atomic geometries than to rectify local moments and spectra, recent success with corrected ionic structures [42–46] encourage us to think of DFT + U as a true correction for ab initio energetics. A linear-scaling implementation of the DFT + U force corrections may be useful, for example, in systems such as biological organometallic complexes, where GGA functionals may tend to systematically overbind ligands to transition-metal ions. As such, we have implemented the DFT + U forces terms, as well as the total-energy minimisation scheme, in the ONETEP code. We shall now describe the required methodology.

We assume that the ground-state density for a given ionic configuration is located before the forces are computed, so that the total-energy is variationally minimised with respect to both the NGWF expansion coefficients and the matrix elements of the density kernel.

The DFT + U correction then contributes to the ionic forces only via the spatial dependence of the Hubbard projection operators, that is for the ion labelled j ,

$$\mathbf{F}_j = -\frac{\partial E_{DFT+U}}{\partial \mathbf{R}_j} = -\sum_J \frac{\partial E_{DFT+U}}{\partial P_{\xi\tau}^{(J)}} \frac{\partial P_{\xi\tau}^{(J)}}{\partial \mathbf{R}_j}. \quad (2.62)$$

In this expression, since the Hubbard projectors are usually considered to be associated with one atomic site only, the subspace index J need only run over subspaces

centred on ion j only. We will henceforth suppress the summation symbol, for notational clarity, since the generalisation to multiple subspaces per ion is straightforward.

The spatial derivative of the NGWF representation of the Hubbard projection operator may be expressed as a spatial derivative of the (real-valued) covariant projectors and contravariant subspace metric tensor themselves. First, however, we define the NGWF representation of the spatial derivative of the Hubbard projectors as the three-component vector

$$\begin{aligned} \mathbf{X}_{\xi m}^{(J)} &= \langle \phi_{\xi} | \nabla | \varphi_m^{(J)} \rangle \\ &= \int d\mathbf{r} \phi_{\xi}(\mathbf{r}) \left[\int d\mathbf{G} (-i\mathbf{G}) e^{-i\mathbf{G}\cdot\mathbf{r}} \varphi_m^{(J)}(\mathbf{G}) \right], \end{aligned} \quad (2.63)$$

and $\mathbf{Y}_{m\xi}^{(J)} = \mathbf{X}_{\xi m}^{(J)}$ is its transpose for each component. The required projection derivative is thus given by

$$\begin{aligned} \frac{\partial P_{\xi\tau}^{(J)}}{\partial \mathbf{R}_j} &= \left(\frac{\partial P_{\xi\tau}^{(J)}}{\partial \varphi_m^{(J)}(\mathbf{r})} \right) \frac{\partial \varphi_m^{(J)}(\mathbf{r})}{\partial \mathbf{R}_j} + \left(\frac{\partial P_{\xi\tau}^{(J)}}{\partial O^{(J)mm'}} \right) \frac{\partial O^{(J)mm'}}{\partial \mathbf{R}_j} \\ &= \int \left(\frac{\partial}{\partial \varphi_m^{(J)}(\mathbf{r})} \left[V_{\xi m'}^{(J)} O^{(J)m'm''} W_{m''\tau}^{(J)} \right] \right) \\ &\quad \times \frac{\partial}{\partial \mathbf{R}_j} \left[\int d\mathbf{G} e^{-i\mathbf{G}\cdot\mathbf{r}} \varphi_m^{(J)}(\mathbf{G}) \right] d\mathbf{r} \\ &= \int \left(\phi_{\xi}(\mathbf{r}) O^{(J)mm''} W_{m''\tau}^{(J)} + V_{\xi m'}^{(J)} O^{(J)m'm} \phi_{\tau}(\mathbf{r}) \right) \\ &\quad \times \left[\int d\mathbf{G} (-i\mathbf{G}) e^{-i\mathbf{G}\cdot\mathbf{r}} \varphi_m^{(J)}(\mathbf{G}) \right] d\mathbf{r} \\ &= \mathbf{X}_{\xi m}^{(J)} O^{(J)mm''} W_{m''\tau}^{(J)} + V_{\xi m'}^{(J)} O^{(J)m'm} \mathbf{Y}_{m\tau}^{(J)}. \end{aligned} \quad (2.64)$$

Here, we have neglected the term involving the partial derivative of the metric tensor with respect to ionic positions, as it vanishes for the localised subspace representation we use here and which we go on to discuss in more detail in [Chap. 4](#). The neglect of this term is appropriate when using either conventional atom-centred system-independent Hubbard projectors or the self-consistently determined variety which we describe in [Chap. 3](#) and Ref. [25], since a rigid displacement of all Hubbard projectors for a correlated subspace does not change the metric tensor on that subspace.

Combining this expression with the result of Eq. 2.57, in order to evaluate the force expression of Eq. 2.62, we conclude that the tensorially consistent DFT+ U contribution to the ionic forces is given, again simplifying using the real-valued nature of both Hubbard projectors and NGWFs, by the easily-evaluated trace of sparse matrices

$$\mathbf{F}_j = -2\mathbf{X}_{\xi m}^{(J)} O^{(J)mm''} W_{m''\tau}^{(J)} H_{\tau\xi}^{(J)DFT+U} \tilde{K}^{\zeta\xi}. \quad (2.65)$$

2.7 Scaling Tests on Nickel Oxide Nano-Clusters

The first row transition-metal monoxide NiO has, for some considerable time, posed difficulties to Kohn–Sham density-functional theory and to electronic structure theories generally. As such, it has served as a valuable proving-ground for novel approaches such as periodic unrestricted Hartree-Fock theory [47], the self-interaction corrected local density approximation [19], the GW approximation [48], LDA + DMFT [49] and first-principles methods for calculating the Hubbard U parameter [16, 50] in DFT + U .

Experimentally, the paramagnetic phase of NiO is found to possess a rock-salt crystal structure with a lattice constant of approximately 4.17 Å [10]. At ambient temperature, NiO is a type-II antiferromagnetic insulator with a local magnetic moment of between 1.64 and 1.9 μ_B [16], with a Néel temperature of approximately 523 K [9].

Due to the persistence of the magnetic moment and the optical gap, which lies at approximately 4 eV, of this material above the Néel temperature, it falls broadly into the category of a Mott insulator [47]. However, the material has been somewhat reclassified as a charge-transfer insulator since experimental data has shown that the states close to the top of the valence band possess a predominantly oxygen $2p$ character while those in the conduction band are of nickel $3d$ -orbital character [51].

Irrespective of nomenclature, it has long been recognised that LDA-type exchange correlation functionals [8] qualitatively fail to reproduce the physics of this material, grossly under-estimating the local magnetic moment, the Kohn–Sham gap (if it is imbued with a physical interpretation) and assigning an incorrect fully $3d$ -orbital character to the valence band edge, but that the DFT + U method successfully corrects these deficiencies [10, 16, 21, 50, 52].

2.7.1 Computational Methodology

We performed scaling tests on NiO nano-clusters of varying size, comparing the computational effort required for DFT + U and uncorrected DFT calculations. We have chosen approximately spherical nano-clusters with an even number of nickel ions, so that we may tentatively assume an open-shell singlet multiplicity, analogous to the bulk antiferromagnetic ground state. In fact, however, we might expect that a transition to a ferrimagnetic or ferromagnetic ground state occurs below some critical cluster size, as it has been predicted for very small iron oxide clusters of interest for data-storage technology [53, 54].

While it is certainly of worthwhile to explore this possibility further using linear-scaling DFT + U , it exceeded the scope of this study, since the spin multiplicity has no direct bearing on computational expense. Moreover, since calculations on nano-clusters of varying sizes may be expected to exhibit differing convergence behaviour, we simply ran the energy-minimisation algorithm for a fixed number of iterations

and did not attempt to achieve the ground-state. In [Chap. 4](#), published in Ref. [27], we return to this material in its bulk form, addressing the DFT+ U description of its physical properties in detail.

2.7.2 *Scaling of Computational Effort for DFT+ U*

A moderate set of run-time parameters was used, since our principal interest was to test the increase in effort needed when the DFT+ U functionality was included in the calculation. These parameters included a 500 eV equivalent plane-wave cutoff energy, a spin-polarised density kernel, the LSDA XC functional [8], a 25 a_0 density kernel cutoff with 7.5 a_0 NGWF cutoff radii, nine NGWFs for each nickel ion and 4 each for oxygen. A fixed number of one NGWF update step and three density kernel update steps, with three penalty-functional idempotency corrections per density kernel update step, were used to test the scaling behaviour without the dependence of convergence behaviour on system size. NGWF overlap matrix inversion was carried out using Hotelling’s algorithm [55] and a cubic simulation super-cell of three times the diameter of each nano-cluster was used, up to a maximum super-cell size of approximately 300 a_0 . Hydrogenic projectors of the type discussed in [Chap. 3](#) were used for DFT+ U .

Figure 2.2 shows computational timing data for ONETEP energy-minimisation of selected NiO nano-clusters containing up to 7,153 atoms on 300 nodes of a commodity supercomputer. A reasonable linear fit was obtained in spite of the rather small number of data points available; the available memory was exceeded when attempting calculations of a larger cluster of 11,513 atoms. The zero-time intercept lay at 450–500 atoms, indicating very efficient initialisation of the pre-requisite data in these calculations.

The NiO nano-clusters are by no means a favourable case for the DFT+ U method, since approximately half of the ions host correlated subspaces. Nonetheless, we see a very small increase in computational time when the DFT+ U functionality is applied, of approximately 5%, and preservation of linear-scaling performance.

Figure 2.3 shows the time spent computing the DFT+ U projection operator and its contribution to the total-energy and Hamiltonian. This indicates that no aspect of this functionality appreciably deviates from linear-scaling behaviour. Also shown is the timing for one calculation of the DFT+ U contribution to the ionic forces, also exhibiting favourable scaling for those calculations which fell within memory resources. Significantly, however, we note that the total time spent in these subroutines makes up only a small fraction of the increase in cost incurred by DFT+ U , remaining at less than 1% of the total computational time.

In order to understand where the dominant contribution to the additional cost originates, if not in the DFT+ U subroutines themselves, we direct the reader to [Fig. 2.4](#), where the size-dependent sparsity of some important matrices, with and without DFT+ U , is quantified.

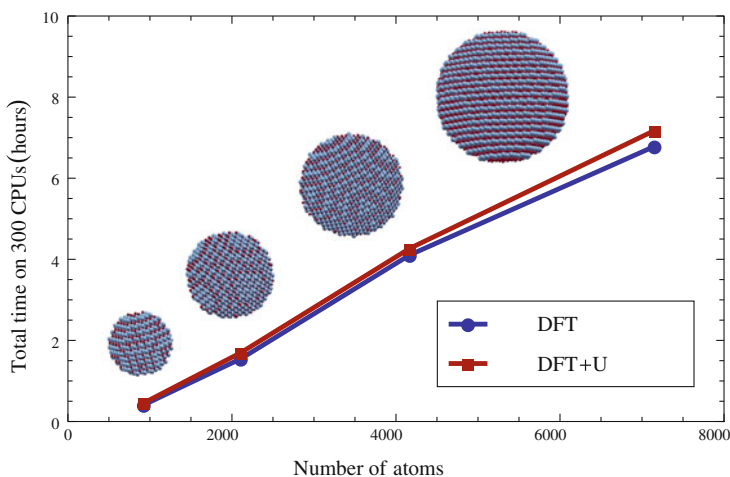


Fig. 2.2 Scaling tests of energy-minimisation functionality, including three density kernel optimisation steps and one NGWF update step, comparing DFT and DFT + U . Four sizeable nano-clusters of NiO were tested on 300 processing cores

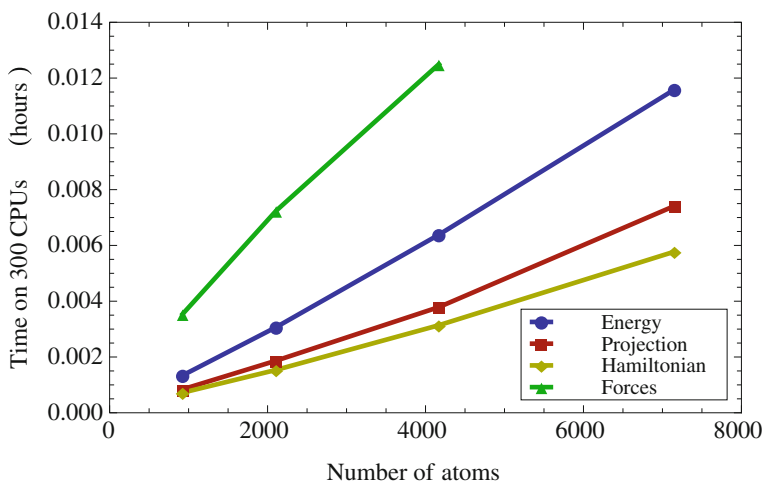


Fig. 2.3 Timing of the DFT + U subroutines in the test calculations shown in Fig. 2.2

For a conventional DFT calculation, the sparsity of the Hamiltonian matrix is dominated by the NGWF representation of the non-local pseudopotential. This in turn is computed using the product of the overlap matrix between the NGWFs and the non-local pseudopotential projectors with its transpose. In essence, pairs of NGWFs which overlap with a common non-local projector must be represented in the Hamiltonian, and the same is true of pairs of NGWFs overlapping with a common Hubbard projector when DFT + U is used.

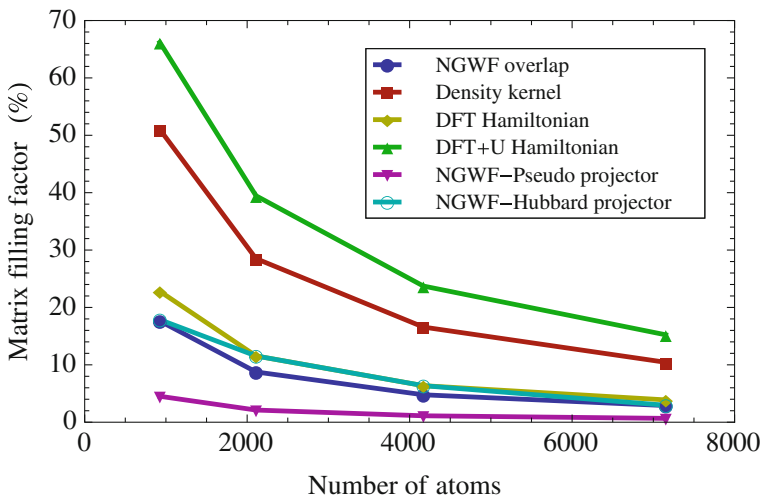


Fig. 2.4 Nano-cluster size dependence of filling factors of principal matrices. These matrix fillings partially determine the computational cost for DFT and DFT+ U

Non-local pseudopotential projectors tend to have radii not in excess of $2 a_0$ for lighter elements, up to and including the first-row transition metals. However, the Hubbard projectors may require radii significantly greater than this, as indicated by the Hubbard projector density shown in Fig. 3.1 for $3d$ -type projectors.

In our implementation of DFT+ U , we attributed a cutoff radius to all Hubbard projectors equal to the NGWF cutoff radii of their host ions, in this case $7.5 a_0$. This was primarily to allow the use of self-consistently determined Hubbard projectors in the form of NGWFs, as we go on to discuss in Chap. 3. When using hydrogenic projectors of smaller characteristic radii, it is almost certainly sufficient to use reduced Hubbard projector cutoff radii for computational efficiency, but we did not explore this possibility. The significant increase in the filling of the Hamiltonian matrix in DFT+ U over DFT, and thus the computation of its products with other quantities such as the density kernel, is thus largely responsible for the incurred increase in computational expense. The increased Hamiltonian filling has consequences too for the calculation of the gradient of the energy with respect to the NGWF expansion coefficients, as indicated in Fig. 2.5, which shows the fractional increase in time spent in some principal operations in the energy-minimisation algorithm.

Due to the increase in the number of matrix elements in the Hamiltonian when the DFT+ U contribution is included, it takes close to twice as much effort to calculate its expansion on the *psinc* grid. Moreover, since the grid-expansion of the action of the Hamiltonian on the NGWFs is also required for the energy gradient with respect to NGWFs, this too is made more costly by DFT+ U .

Of course, when using hydrogenic Hubbard projectors, at least for first-row transition metal ions, we could safely reduce the cutoff radii of the Hubbard projectors and

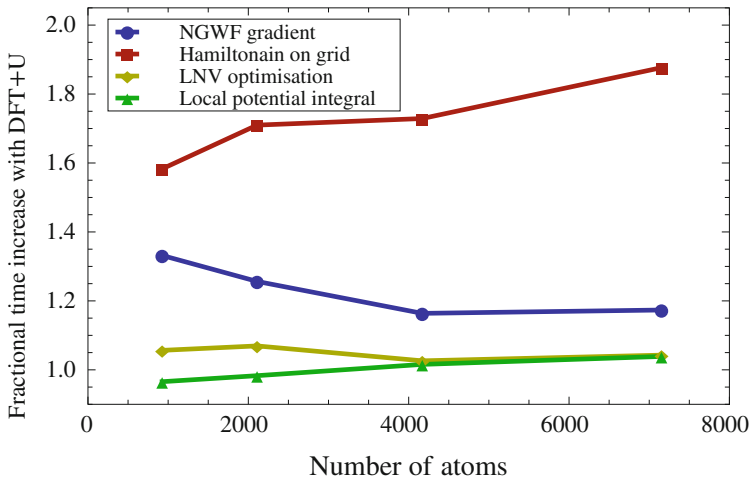


Fig. 2.5 Fractional increase in time spent on selected operations when the DFT + U functionality is activated

therefore the number of matrix elements included in the Hamiltonian, if so desired. If carried out, this would be expected to further reduce the increase in linear-scaling pre-factor for these systems from approximately 5% closer to the much lower fraction which is purely due to the DFT + U subroutines.

2.8 Concluding Remarks

We have detailed a linear-scaling implementation of the widely-used DFT + U method for treating strongly-correlated systems from first-principles. The formalism is generally appropriate to methods which minimise the energy with respect to the single-particle density-matrix, and allows for the optimisation of a nonorthogonal representation, nonorthogonal Hubbard projectors and ionic positions.

We have demonstrated the preservation of linear-scaling performance on strongly-correlated nano-clusters in excess of 7,000 atoms. Even for systems such as these, with a high density of correlated sites, the increase in computational pre-factor is rather modest. The method is, furthermore, expected to incur negligible extra cost in large systems comprising only a small number of Hubbard subspaces.

We expect that our method may be helpful in bringing linear-scaling DFT to bear on more problematic systems than those to which it is usually applied, for example binding-sites in organometallic enzymes, heterostructures containing magnetic layers for data storage and processing, defective oxides and interfaces with catalytic oxide surfaces.

References

1. J.A. Pople, R.K. Nesbet, Self-consistent orbitals for radicals. *J. Chem. Phys.* **22**, 572 (1954)
2. P. Hohenberg, W. Kohn, Inhomogeneous electron gas. *Phys. Rev.* **136**(3B), B864 (1964)
3. W. Kohn, L.J. Sham, Self-consistent equations including exchange and correlation effects. *Phys. Rev.* **140**(4A), A1133 (1965)
4. J.S. Miller, A.J. Epstein, Organic and organometalling molecular magnetic materials—designer magnets. *Angew. Chem. Int. Ed. Engl.* **33**, 385 (1994)
5. B.C.H. Steele, A. Heinzl, Materials for fuel-cell technologies. *Nature* **414**, 345 (2001)
6. R.H. Holm, P. Kennepohl, E.I. Solomon, Structural and functional aspects of metal sites in biology. *Chem. Rev.* **96**, 2239 (1996)
7. N.F. Mott, The basis of the electron theory of metals, with special reference to the transition metals. *Proc. Phys. Soc. A* **62**, 416 (1949)
8. J.P. Perdew, A. Zunger, Self-interaction correction to density-functional approximations for many-electron systems. *Phys. Rev. B* **23**(10), 5048 (1981)
9. K. Terakura, T. Oguchi, A.R. Williams, J. Kübler, Band theory of insulating transition-metal monoxides: Band-structure calculations. *Phys. Rev. B* **30**(8), 4734 (1984)
10. S.L. Dudarev, G.A. Botton, S.Y. Savrasov, C.J. Humphreys, A.P. Sutton, Electron-energy-loss spectra and the structural stability of nickel oxide: an LSDA+U study. *Phys. Rev. B* **57**(3), 1505 (1998)
11. J. Hubbard, Electron correlations in narrow energy bands. *Proc. R. Soc. London Ser. A* **276**, 238 (1963)
12. J. Hubbard, Electron correlations in narrow energy bands II: the degenerate band case. *Proc. R. Soc. London Ser. A* **277**, 237 (1964)
13. J. Hubbard, Electron correlations in narrow energy bands III: an improved solution. *Proc. R. Soc. London Ser. A* **281**, 401 (1964)
14. E. Artacho, del L.M. Bosch, Nonorthogonal basis sets in quantum mechanics: representations and second quantization. *Phys. Rev. A* **43**(11), 5770 (1991)
15. J.P. Perdew, R.G. Parr, M. Levy, J.L. Balduz, Density-functional theory for fractional particle number: derivative discontinuities of the energy. *Phys. Rev. Lett.* **49**(23), 1691 (1982)
16. M. Cococcioni, de S. Gironcoli, Linear response approach to the calculation of the effective interaction parameters in the LDA+U method. *Phys. Rev. B* **71**(3), 035105 (2005)
17. H.J. Kulik, M. Cococcioni, D.A. Scherlis, N. Marzari, Density functional theory in transition-metal chemistry: a self-consistent Hubbard U approach. *Phys. Rev. Lett.* **97**(10), 103001 (2006)
18. A.J. Cohen, P. Mori-Sanchez, W. Yang, Insights into current limitations of density functional theory. *Science* **321**(5890), 792 (2008)
19. A. Svane, O. Gunnarsson, Transition-metal oxides in the self-interaction-corrected density-functional formalism. *Phys. Rev. Lett.* **65**(9), 1148 (1990)
20. V.I. Anisimov, J. Zaanen, O.K. Andersen, Band theory and Mott insulators: Hubbard U instead of Stoner I. *Phys. Rev. B* **44**(3), 943 (1991)
21. V.I. Anisimov, I.V. Solovyev, M.A. Korotin, M.T. Czyżyk, G.A. Sawatzky, Density-functional theory and NiO photoemission spectra. *Phys. Rev. B* **48**(23), 16929 (1993)
22. V.I. Anisimov, A.I. Poteryaev, M.A. Korotin, A.O. Anokhin, G. Kotliar, First-principles calculations of the electronic structure and spectra of strongly correlated systems: dynamical mean-field theory. *J. Phys. Condens. Matter* **9**(35), 7359 (1997)
23. A.I. Lichtenstein, M.I. Katsnelson, Ab initio calculations of quasiparticle band structure in correlated systems: LDA++ approach. *Phys. Rev. B* **57**(12), 6884 (1998)
24. S. Atwell, E. Meggers, G. Spraggon, P.G. Schultz, Structure of a copper-mediated base pair in DNA. *J. Am. Chem. Soc.* **123**(49), 12364 (2001)
25. D.D. O'Regan, N.D.M. Hine, M.C. Payne, A.A. Mostofi, Projector self-consistent DFT+U using nonorthogonal generalized Wannier functions. *Phys. Rev. B* **82**(8), 081102 (2010)

26. L.V. Pourovskii, B. Amadon, S. Biermann, A. Georges, Self-consistency over the charge density in dynamical mean-field theory: a linear muffin-tin implementation and some physical implications. *Phys. Rev. B* **76**(23), 235101 (2007)
27. D.D. O'Regan, M.C. Payne, A.A. Mostofi, Subspace representations in ab initio methods for strongly correlated systems. *Phys. Rev. B* **83**(24), 245124 (2011)
28. V.I. Anisimov, F. Aryasetiawan, A.I. Lichtenstein, First-principles calculations of the electronic structure and spectra of strongly correlated systems: the LDA + U method. *J. Phys. Condens. Matt.* **9**(4), 767 (1997)
29. A.I. Liechtenstein, V.I. Anisimov, J. Zaanen, Density-functional theory and strong interactions: orbital ordering in Mott–Hubbard insulators. *Phys. Rev. B* **52**(8), R5467 (1995)
30. M.T. Czyżyk, G.A. Sawatzky, Local-density functional and on-site correlations: the electronic structure of La_2CuO_4 and LaCuO_3 . *Phys. Rev. B* **49**(20), 14211 (1994)
31. D.-K. Seo, Self-interaction correction in the LDA + U method. *Phys. Rev. B* **76**, 033102 (2007)
32. R. McWeeny, Some recent advances in density matrix theory. *Rev. Mod. Phys.* **32**(2), 335 (1960)
33. X.-P. Li, R.W. Nunes, D. Vanderbilt, Density-matrix electronic-structure method with linear system-size scaling. *Phys. Rev. B* **47**(16), 10891 (1993)
34. R.W. Nunes, D. Vanderbilt, Generalization of the density-matrix method to a nonorthogonal basis. *Phys. Rev. B* **50**(23), 17611 (1994)
35. M.S. Daw, Model for energetics of solids based on the density matrix. *Phys. Rev. B* **47**(16), 10895 (1993)
36. P.D. Haynes, C.-K. Skylaris, A.A. Mostofi, M.C. Payne, Density kernel optimization in the ONETEP code. *J. Phys. Condens. Matt.* **20**(29), 294207 (2008)
37. C.A. White, P. Maslen, M.S. Lee, M. Head-Gordon, The tensor properties of energy gradients within a non-orthogonal basis. *Chem. Phys. Lett.* **276**(1–2), 133 (1997)
38. F. Mauri, G. Galli, R. Car, Orbital formulation for electronic-structure calculations with linear system-size scaling. *Phys. Rev. B* **47**(15), 9973 (1993)
39. F. Mauri, G. Galli, Electronic-structure calculations and molecular-dynamics simulations with linear system-size scaling. *Phys. Rev. B* **50**(7), 4316 (1994)
40. J. Kim, F. Mauri, G. Galli, Total-energy global optimizations using nonorthogonal localized orbitals. *Phys. Rev. B* **52**(3), 1640 (1995)
41. P. Ordejón, D.A. Drabold, R.M. Martin, M.P. Grumbach, Linear system-size scaling methods for electronic-structure calculations. *Phys. Rev. B* **51**(3), 1456 (1995)
42. D.A. Scherlis, M. Cococcioni, P. Sit, N. Marzari, Simulation of heme using DFT + U: a step toward accurate spin-state energetics. *J. Phys. Chem. B* **111**(25), 7384 (2007)
43. H.J. Kulik, N. Marzari, A self-consistent Hubbard U density-functional theory approach to the addition–elimination reactions of hydrocarbons on bare FeO^+ . *J. Chem. Phys.* **129**(13), 134314 (2008)
44. H.J. Kulik, N. Marzari, Systematic study of first-row transition-metal diatomic molecules: a self-consistent DFT + U approach. *J. Chem. Phys.* **133**(11), 114103 (2010)
45. H.J. Kulik, L.C. Blasiak, N. Marzari, C.L. Drennan, First-principles study of non-heme Fe(II) halogenase SyrB2 reactivity. *J. Am. Chem. Soc.* **131**(40), 14426 (2009)
46. H. Hsu, K. Umemoto, M. Cococcioni, R. Wentzcovitch, First-principles study for low-spin LaCoO_3 with a structurally consistent Hubbard U. *Phys. Rev. B* **79**(12), 125124 (2009)
47. M.D. Towler, N.L. Allan, N.M. Harrison, V.R. Saunders, W.C. Mackrodt, E. Aprà, Ab initio study of MnO and NiO . *Phys. Rev. B* **50**(8), 5041 (1994)
48. F. Aryasetiawan, O. Gunnarsson, Electronic structure of NiO in the GW approximation. *Phys. Rev. Lett.* **74**(16), 3221 (1995)
49. X. Ren, I. Leonov, G. Keller, M. Kollar, I. Nekrasov, D. Vollhardt, LDA + DMFT computation of the electronic spectrum of NiO . *Phys. Rev. B* **74**(19), 195114 (2006)
50. W.E. Pickett, S.C. Erwin, E.C. Ethridge, Reformulation of the LDA + U method for a local-orbital basis. *Phys. Rev. B* **58**(3), 1201 (1998)

51. G.A. Sawatzky, J.W. Allen, Magnitude and origin of the band gap in NiO. *Phys. Rev. Lett.* **53**(24), 2339 (1984)
52. O. Bengone, M. Alouani, P. Blöchl, J. Hugel, Implementation of the projector augmented-wave LDA+U method: application to the electronic structure of NiO. *Phys. Rev. B* **62**(24), 16392 (2000)
53. S. López, A.H. Romero, J. Mejía-López, J. Mazo-Zuluaga, J. Restrepo, Structure and electronic properties of iron oxide clusters: a first-principles study. *Phys. Rev. B* **80**(8), 085107 (2009)
54. K. Palotás, A.N. Andriotis, A. Lappas, Structural, electronic, and magnetic properties of nanometer-sized iron-oxide atomic clusters: comparison between GGA and GGA+U approaches. *Phys. Rev. B* **81**(7), 075403 (2010)
55. T. Ozaki, Efficient recursion method for inverting an overlap matrix. *Phys. Rev. B* **64**(19), 195110 (2001)

Optimised Projections for the Ab Initio Simulation of
Large and Strongly Correlated Systems

O'Regan, D.D.

2012, XVI, 216 p., Hardcover

ISBN: 978-3-642-23237-4